Computational and Structural Biotechnology Journal 22 (2023) 3–16

Contents lists available at ScienceDirect

Computational and Structural Biotechnology Journal

journal homepage: www.elsevier.com/locate/csbj

Research article

Continuous shared control of a mobile robot with brain–computer interface and autonomous navigation for daily assistance☆

Baoguo Xu [a,*], Deping Liu [a], Muhui Xue [a], Minmin Miao [b], Cong Hu [c], Aiguo Song [a]

[a] State Key Laboratory of Bioelectronics, Jiangsu Key Laboratory of Remote Measurement and Control, School of Instrument Science and Engineering, Southeast University, Nanjing 210096, China
[b] School of Information Engineering, Huzhou University, Huzhou 313000, China
[c] Guangxi Key Laboratory of Automatic Detecting Technology and Instruments, Guilin University of Electronic Technology, Guilin 541004, China

ARTICLE INFO

Keywords:
Brain—computer interface (BCI)
Continuous shared control
Mobile robot
Motor
Imagery (MI)

ABSTRACT

Although the electroencephalography (EEG) based brain–computer interface (BCI) has been successfully developed for rehabilitation and assistance, it is still challenging to achieve continuous control of a brain-actuated mobile robot system. In this study, we propose a continuous shared control strategy combining continuous BCI and autonomous navigation for a mobile robot system. The weight of shared control is designed to dynamically adjust the fusion of continuous BCI control and autonomous navigation. During this process, the system uses the visual-based simultaneous localization and mapping (SLAM) method to construct environmental maps. After obtaining the global optimal path, the system utilizes the brain-based shared control dynamic window approach (BSC-DWA) to evaluate safe and reachable trajectories while considering shared control velocity. Eight subjects participated in two-stage training, and six of these eight subjects participated in online shared control experiments. The training results demonstrated that naïve subjects could achieve continuous control performance with an average percent valid correct rate of approximately 97 % and an average total correct rate of over 80 %. The results of online shared control experiments showed that all of the subjects could complete navigation tasks in an unknown corridor with continuous shared control. Therefore, our experiments verified the feasibility and effectiveness of the proposed system combining continuous BCI, shared control, autonomous navigation, and visual SLAM. The proposed continuous shared control framework shows great promise in BCI-driven tasks, especially navigation tasks for brain-driven assistive mobile robots and wheelchairs in daily applications.

1. Introduction

A brain–computer interface (BCI) directly connects the brain with external devices by converting neural signals into interactive instructions. Therefore, a BCI can provide alternative links to replace natural links disrupted by diseases or injuries. In recent years, advanced BCI systems have shown great promise in assistance and rehabilitation for both healthy users and people with neurological disorders such as amyotrophic lateral sclerosis (ALS) [1]. These systems enable users to perform effective training and interactive tasks through brain-driven external devices. A series of studies have shown the great potential of electroencephalogram (EEG)-based BCI systems in control applications, including the control of virtual cursors [2], robotic arms [3], and mobile robotic platforms such as wheelchairs [4]. Event-related desynchronization (ERD) and event-related synchronization (ERS) on sensorimotor rhythms (SMR) are generated spontaneously in motor imagery (MI) tasks [5,6], and they can be detected and decoded by an MI-based paradigm. MI-based paradigms obtain control instructions consistent

☆ This work was supported in part by the National Key Research and Development Program of China under Grant 2022YFC2405602, in part by the Natural Science Foundation of Jiangsu Province, under Grant BK20221464, in part by the Key Research and Development Program of Jiangsu Province, under Grant BE2022363, in part by the Basic Research Project of Leading Technology of Jiangsu Province, under Grant BK20192004, in part by the National Natural Science Foundation of China, under Grants 92148205, 62173088, and 62173089 and in part by the Guangxi Key Laboratory of Automatic Detecting Technology and Instruments under Grant YQ22207. The studies involving human participants were reviewed and approved by Ethics Committee of Southeast University. The participants provided their written informed consent to participate in this study.

* Corresponding author.
E-mail address: xubaoguo@seu.edu.cn (B. Xu).

https://doi.org/10.1016/j.csbj.2023.07.033
Received 7 May 2023; Received in revised form 4 July 2023; Accepted 22 July 2023
Available online 29 July 2023

with the user's intention and have been widely used in control systems [7–9].

In most MI-based BCI systems, the user's intentions are classified as discrete high-level control commands, and BCI systems trigger predetermined instructions in the workspace through discrete decoding frameworks, including subtasks and direction selection [3,10]. Although well-trained decoders have improved the efficiency of online control, using a discrete paradigm does not allow for natural and precise control. A few studies have investigated the performance and promise of continuous BCI output as a control signal for robotic devices. Continuous control of a virtual cursor was realized in one-dimensional (1D) [11] and two-dimensional (2D) positions [12] based on regressing SMR signals, and a series of experiments on healthy subjects and disabled patients were carried out to verify the feasibility of the method. Furthermore, continuous SMR-based control frameworks of robotic arms have been proposed for reach and grasp tasks [9] and continuous tracking tasks [13,14]. These studies have demonstrated the feasibility of task training for users and continuous control of robotic devices based on MI EEG. Despite the great efforts made to integrate BCI and robotic arms, continuous control of mobile platforms (such as wheelchairs) through neural modulations does not yet feel completely natural for most users. Compared with fixed robotic arms, the continuous control of MI-based mobile robot systems enables users to interact with a wider area naturally and is of great significance in daily assistance.

Most brain-actuated mobile systems focus on obtaining functional instructions through EEG. Current research mainly uses BCI to achieve discrete directional or angular outputs [7,15] or hierarchical task selection [8]. In a recent MI-based mobile robot study, the 2-class BCI method was used to implement left and right turns constrained by a polar polynomial trajectory strategy [10]. With this method, although users exert high-level control through discrete diagrams, the control process is still somewhat guided by robotic autonomy, thereby limiting the engagement of users. Another study on continuous BCI control designed a dynamic control framework based on a Gaussian classifier [16]. Unfortunately, limited by unknown environmental barriers and the number of independent MI-induced signals, driving a mobile robot continuously and directly through BCI creates an unacceptably heavy mental workload for the user [15]. To improve the stability and performance of brain-driven systems, shared control has been used to combine BCI commands and robotic autonomous intelligence [17]. Shared control is a control strategy that combines human control intention and robotic autonomous intelligence and can adapt to environmental changes, allowing users to participate in the interaction more effectively and with less workload [18]. Shared control arbitrators have been designed to use fixed weights [3], distance-based weights [19], and other methods [20,21] to fuse different control signals. These studies have demonstrated that the adoption of shared control could take advantage of human intention and robotic autonomous intelligence to improve the performance of BCI systems in a complex environment. However, the arbitrator is typically designed based on specific tasks. Exploring the design of an adaptive shared control strategy is a worthwhile pursuit to prevent unstable control switches and offer flexible interaction rules.

In shared control frameworks, autonomous robotic perception and planning provide important assistance for continuous BCI paradigms [22,23]. Unknown environments are common workspaces for brain-driven mobile robot systems. Thus, self-localizing and environmental sensing are valuable capabilities for intelligent BCI systems in navigation tasks [10]. Simultaneous localization and mapping (SLAM) can reconstruct an environmental map while also obtaining the localization of a robot in parallel [24]. Three-dimensional (3D) dense maps can aid control and navigation in unknown environments. Despite this, driving a mobile robot through continuous BCI can still be challenging due to nonstationary EEG patterns and motion constraints. Satisfying the nonholonomic constraints of a mobile robot is the key to integrating user intention and robotic autonomy continuously. The dynamic window approach (DWA) enables a robot to follow a certain motion constraint and avoid local obstacles [25], and it has been increasingly developed in recent research [26,27]. However, when evaluating sampling trajectories, the cost function of DWA does not consider a dynamic velocity component, which is essential to track a velocity-based control signal in human–robot interaction. Therefore, it is necessary to design a velocity-related evaluation component to provide a locally reachable and collision-free trajectory generated by the required velocity.

In the present study, to achieve continuous shared control with dynamic adaptation to environmental changes based on BCI, we developed a brain-actuated mobile robot system consisting of EEG-based teleoperation, visual SLAM, continuous shared control, and autonomous navigation. To the best of our knowledge, this study is the first to combine continuous BCI, visual SLAM, shared control, and autonomous navigation to realize the continuous shared control of a mobile robot in an unknown environment. To summarize the proposed system, first, MI EEG signals are mapped onto continuous linear velocity control signals by an auto-regressive (AR) model. Second, RGB and depth images are input into a visual SLAM method to build environment-dense maps, which are converted into grid maps afterward operation. Third, a weight based on the obstacle potential field is used to fuse continuous EEG velocity and current velocity as shared control velocity. Furthermore, both global and local path planners are used based on the environment grid-based map. This continuous shared control strategy combines continuous BCI control and autonomous navigation. The feasibility of the proposed system was verified by two-stage training and online shared control experiments. This system can be applied in brain-controlled wheelchairs and assistive mobile robots to provide assistance for users with limited mobility.

2. Materials and methods

2.1. System architecture

Fig. 1 presents an overview of the proposed brain-actuated mobile robot system based on continuous BCI control, visual SLAM, shared control, and autonomous navigation. The whole system consists of three components: a BCI module, a mobile robot module, and a planning and control module. For the BCI module, a user-friendly interface was designed for MI EEG signal pre-processing and continuous regression. The BCI module is responsible for displaying visual feedback from the mobile robot module. The function of the mobile robot module is to build an environmental map and obtain the pose transformation matrix. An RGB-D camera provides video feedback and detects information about the surrounding environment, which it inputs to a visual-based SLAM framework. The 3D dense map built by SLAM is converted into a 2D costmap for subsequent planning. The planning and control module intelligently combines continuous BCI commands and global planning commands as velocity constraints to control the mobile robot. Teleoperation is implemented by the transmission of information between different subsystems through TCP/IP.

2.2. Brain–computer interface module

2.2.1. MI EEG acquisition

As shown in Fig. 2, 18 channels (i.e., FC5, FC3, FC1, FC2, FC4, FC6, C5, C3, C1, C2, C4, C6, CP5, CP3, CP1, CP2, CP4, and CP6) of EEG signals were recorded at a sampling frequency of 500 Hz using a Neuroscan SynAmps2 amplifier (Neuroscan Inc., the USA) according to the international 10–20 system. A bandpass filter encompassing 0.5–50 Hz and a notch filter at 50 Hz were applied. The reference electrode and the ground electrode were located on the left mastoid and the forehead, respectively. The impedance of each electrode was kept below 10 kΩ.

2.2.2. Signal processing and regression mapping

A common average reference (CAR) filter was utilized to preprocess

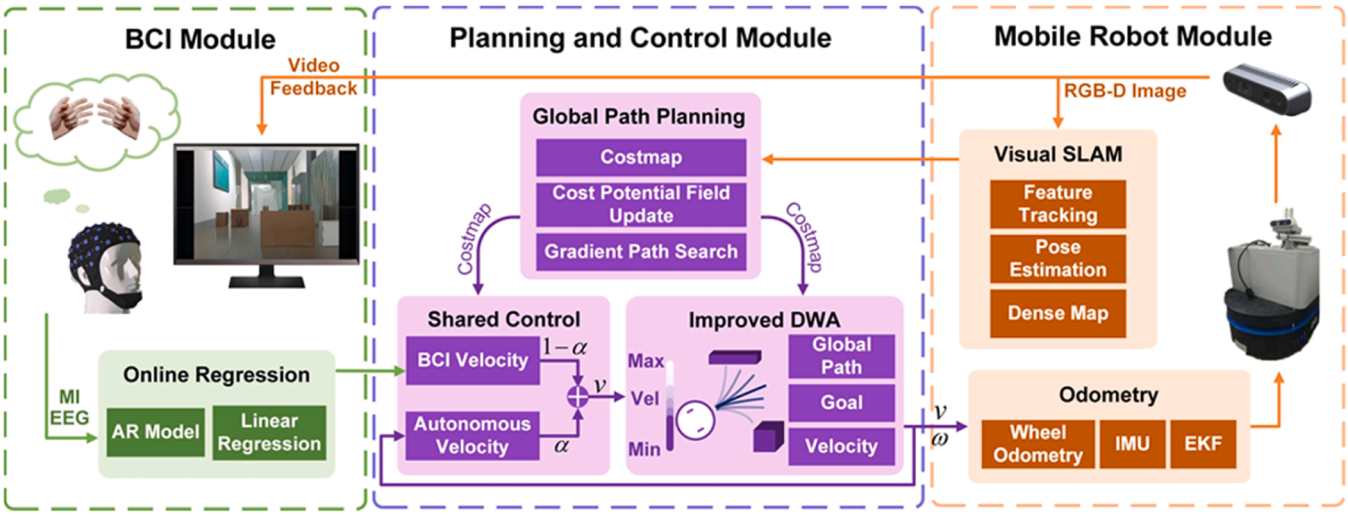

Fig. 1. Overview of the proposed brain-actuated mobile robot system. The system consists of a BCI module, a mobile robot module, and a planning and control module. The subject continuously controls the BCI linear velocity through an MI paradigm in the BCI module. The mobile robot module is responsible for environmental perception and localization. The continuous shared control strategy combining BCI velocity and autonomous velocity is executed in the planning and control module.

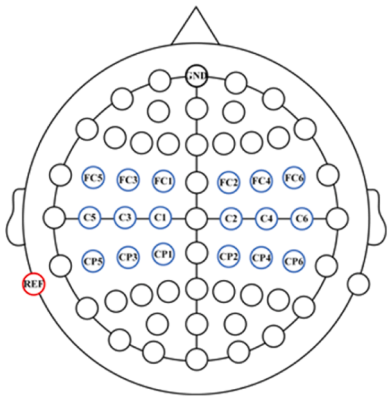

Fig. 2. The positions of electrodes used in this study.

the raw EEG signals. The amplitudes of the EEG signals for each subject were selected to serve as features. A 16-order autoregressive (AR) model [28] was conducted by BCI2000 [29] in the experiment, defined by the following equation:

$$x_t = \sum_{i=1}^{p} a_i x_{t-i} + \varepsilon \tag{1}$$

where x_t is the estimated signal at time t; ε is white noise with a mean of zero; i and p represent the i-th sample and the autoregressive order of the AR model, respectively; and a_i is the AR coefficient, which was estimated based on the least squares criterion.

A linear equation was used to build regressive mapping between EEG signals and the vertical coordinates of the virtual cursor. The vertical movement of the virtual cursor can be described as:

$$K = \omega_R R + \omega_L L + d \tag{2}$$

where K is the vertical coordinate value of the virtual cursor; R and L are the signals of the right and left channels respectively; ω_R and ω_L are weights for the corresponding channels, and they each have an initial value of 1; and d is the offset with an initial value of 0. The amplitude features of selected channels and frequent bands calculated by the AR model were input to the equation,and the weights were dynamically adapted depending on the least mean square (LMS) algorithm.

2.3. Mobile robot module

2.3.1. Nonholonomic-constrained mobile robot model

As illustrated in Fig. 3(a), instead of an omnidirectional mobile robot [30], we used a nonholonomic-constrained mobile robot [22] in this study. The distance between the centers of the two driving wheels was denoted as l. We set the world coordinate system $O_W X_W Y_W Z_W$, and then set O_R as the origin of the robot coordinate system $O_R X_R Y_R Z_R$. The angular and linear velocity of the robot can be described as follows:

$$\omega = \frac{v_r - v_l}{l} \tag{3}$$

$$v = \frac{v_r + v_l}{2} \tag{4}$$

Traditionally, a three-generalized coordinate P can be used to describe the kinematic parameters of a mobile robot. When the robot is in an ideal environment, its kinematic model can be described as follows:

$$P = [x, y, \theta]^T \tag{5}$$

$$\begin{bmatrix} \dot{x} \\ \dot{y} \\ \dot{\theta} \end{bmatrix} = \begin{bmatrix} \cos\theta & 0 \\ \sin\theta & 0 \\ 0 & 1 \end{bmatrix} \begin{bmatrix} v \\ \omega \end{bmatrix} \tag{6}$$

where x, y, and θ represent the abscissa, ordinate, and rotation angle of the mobile robot, respectively.

2.3.2. Visual SLAM module

In an unknown environment, SLAM improves the robot's environmental perception ability without a prior global map. A RealSense D435 RGB-D camera (Intel Inc., USA) fixed on the mobile robot was used to obtain figures and generate a 3D dense map. The proposed method was extended based on the RGB-D version of the ORB-SLAM2 [31] framework.

As shown in Fig. 3(b), when a keyframe was generated, the corresponding pose transformation matrix (including rotation matrix and translation vector) was stored. The keyframes and pose transformation matrix were passed to the point cloud map construction thread. Local point cloud maps were generated for each keyframe.

Point clouds collected by visual SLAM were preprocessed before being input into Octomap. We utilized the Radius Outlier Removal filter

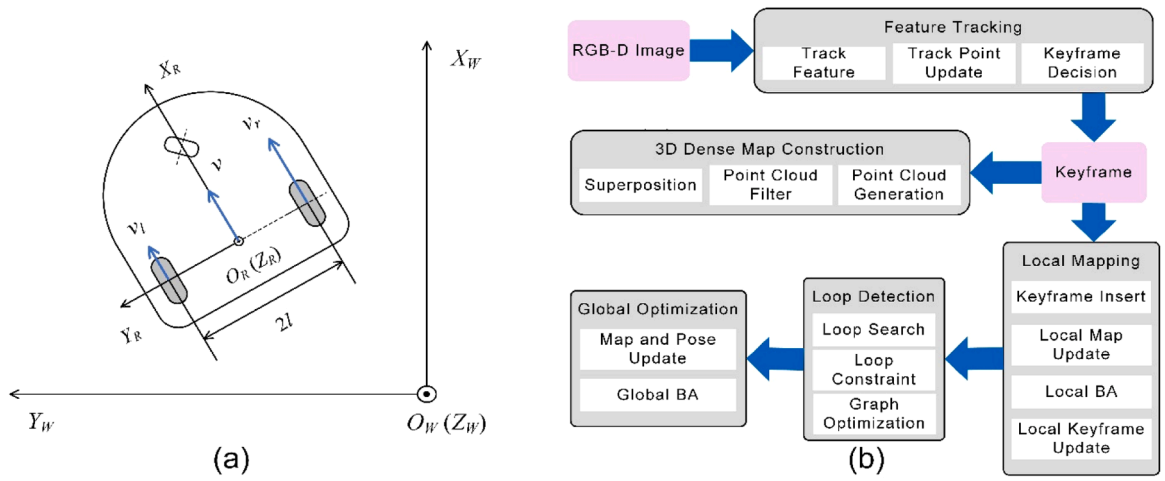

Fig. 3. (a) The platform of the mobile robot used in this study. The mobile robot obeys nonholonomic constraints. (b) The proposed visual SLAM architecture. RGB-D images are input into the visual SLAM to realize map construction and pose estimation.

and voxel grid filter for the removal of outlier points and downsampling.

Fig. 4 shows a sample of the filtered 3D dense map of the corridor environment in online shared control experiments. After the preprocessing, the filtered point clouds were converted into Octomap in ROS and added to its workspace. We used Octomap to generate costmaps to be input into the move_base stack, thus creating a framework for autonomous navigation by enabling the integration of various modules such as global and local planners, obstacle avoidance, and path execution. Output grid maps were divided into multi-layered costmaps using the costmap_2D plugin provided in the ROS Navigation package, and then we employed the extended Kalman filter (EKF) to obtain combined odometry information, which provided a transformation matrix between the map and footprint of the robot for navigation.

2.4. Planning and control module

2.4.1. Global path planner

For a global path planner, it is necessary to obtain information about the surrounding environment to calculate collision-free paths satisfying the motion constraints. Sampling-based planning methods and search-based planning methods are the two main types of global path motion planning methods. We used the Dijkstra algorithm to plan the global path based on potential fields. The planner was implemented by the ROS navigation stack [32].

2.4.2. Continuous shared control on linear velocity

We proposed a continuous and adaptive shared control strategy on linear velocity. To realize the continuous control of linear velocity, the strategy was designed to implement a linear combination of the continuous BCI control output and the linear velocity of the robot with a weight that was automatically tuned according to the environment. The shared control strategy was designed to combine continuous BCI control and autonomous navigation control. This process can be described as follows:

$$v_{sc} = (1-\alpha)v_{bci} + \alpha v_{robot} \tag{7}$$

$$v_{bci} = \frac{K}{K_{\max}} v_{\max} \tag{8}$$

$$\alpha = \begin{cases} \dfrac{C_{\text{cost}} - 1}{C_{\text{cost}}} e^{-\lambda(d_{obs} - R_{inscribed})}, d_{obs} < R_{inflation} \\ 0, d_{obs} \geq R_{inflation} \end{cases} \tag{9}$$

where v_{sc} is the shared control signal; v_{bci} is the continuous BCI control signal; v_{robot} is the linear velocity of the robot; α is the weight allocating the control authority; K and $K_{\max}$ are the vertical coordinates of the cursor defined in (2) and the maximum of vertical coordinates, respectively; $v_{\max}$ is the maximum linear velocity of the mobile robot; C_{cost} is a constant value of the costmap; λ is the scale coefficient, and the larger the value of λ, the faster the cost value changes around the obstacle; d_{obs} is the distance between the obstacle and the center of the mobile robot; $R_{inscribed}$ is the radius of the inscribed circle of the robot's outline; and $R_{inflation}$ is the expansion distance. The parameters of the shared control strategy are listed in Table 1.

Eq. (7) defines the proposed shared control method. Furthermore, Eqs. (8) and (9) define the generation rule of v_{bci} and the relationship between the weight and the cost, respectively. As shown in Eq. (9), the linear velocity was directly controlled by the EEG signal when the distance between the robot and the obstacle was greater than the expansion distance; when the opposite was true, the shared control strategy worked. As demonstrated in Fig. 5(a), a smaller distance between the robot and the obstacle led to a larger shared control weight value. Therefore, the weight of the BCI control signal was decreasing, so the robot system tended to choose the control signals generated by autonomous navigation. This method can dynamically and continuously adjust the influence of different signals in the shared control strategy.

Fig. 4. Sample of filtered 3D dense map of experimental corridor workspace.

Table 1
Parameters of shared control strategy.

Symbol	Value	Symbol	Value	Symbol	Value
$K_{\max}$	4095	C_{cost}	253	λ	10
$v_{\max}$	0.2 m s^{-1}	$R_{inscribed}$	0.2 m	$R_{inflation}$	1.5 m

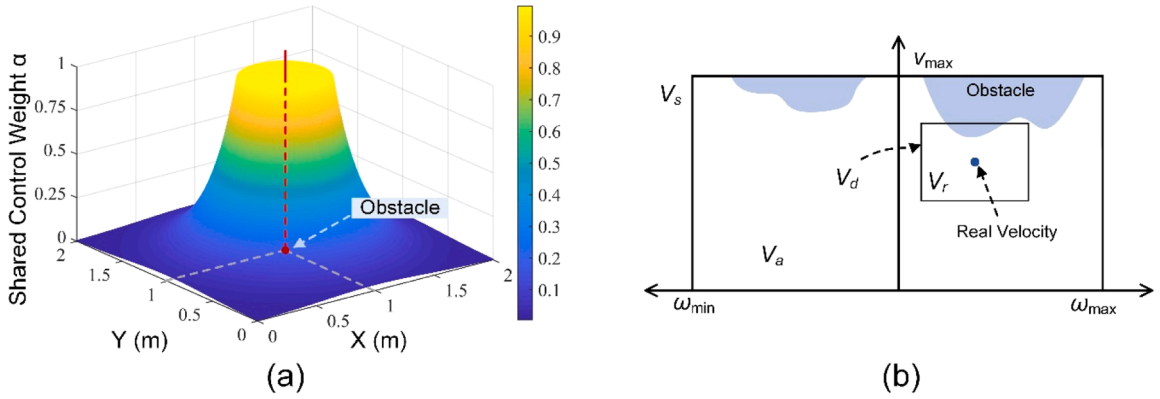

Fig. 5. (a) Distribution diagram of shared control weight around obstacle (1 m, 1 m). The continuous shared control strategy was designed to work when the distance from the obstacle to the robot was smaller than the inflated distance. The shared control weight dynamically adapted to changes in the surrounding environment. (b) Diagram of constrained velocity space.

2.4.3. Shared control-based BSC-DWA local planner

During navigation tasks, global path planning sets the optimal collision-free path for the robot to reach the target from the current position without considering the motion constraints. DWA is one of the local navigation methods [25] widely used in navigation tasks [27,33]. The collision-free path is calculated based on dynamic windows. The velocity space with kinematic constraints is sampled and the simulation trajectory of each sample velocity is evaluated to obtain velocity planning.

In this study, we propose a brain-based shared control DWA (BSC-DWA) method that integrates the shared control-related velocity evaluation component and traditional DWA evaluation components.

First, the pairs (v, ω) are sampled in the velocity space V_r that is obtained by constraints of different velocity subspaces. Fig. 5(b) shows the diagram of velocity spaces used in BSC-DWA. Velocity space V_s contains all of the available velocities and is calculated as follows:

$$V_s = \{(v,\omega)|v \in [v_{\min}, v_{\max}] \wedge \omega \in [\omega_{\min}, \omega_{\max}]\} \tag{10}$$

where $v_{\min}$ and $v_{\max}$ are the minimum and maximum linear velocities, respectively; and $\omega_{\min}$ and $\omega_{\max}$ are the minimum and maximum angular velocities, respectively.

Velocity space V_a contains acceptable velocities at which the robot can stop safely and is calculated as follows:

$$V_a = \left\{ \left(v,\omega\right) \middle| v \le \sqrt{2d_{obs}\dot{v}_b} \wedge \omega \le \sqrt{2d_{obs}\dot{\omega}_b} \right\} \tag{11}$$

where d_{obs} is the closest distance between obstacle and robot; and $\dot{v}_b$ and $\dot{\omega}_b$ are the critical linear acceleration and critical angular acceleration, respectively, at which the robot can stop safely.

Velocity space V_d contains reachable velocities in simulated time and is calculated as follows:

$$\begin{aligned} V_d = \{(v,\omega)|v \in [v_{cur} - \dot{v}t, v_{cur} + \dot{v}t] \\ \wedge\omega \in [\omega_{cur} - \dot{\omega}t, \omega_{cur} + \dot{\omega}t]\} \end{aligned} \tag{12}$$

where v_{cur} and ω_{cur} are current linear velocities and angular velocities, respectively; $\dot{v}$ and $\dot{\omega}$ are the linear acceleration and angular acceleration, respectively; and t represents the simulated time.

Thus, velocity space V_r is restricted by the abovementioned subspaces as follows:

$$V_r = V_s \cap V_a \cap V_d \tag{13}$$

Then, simulated trajectories are generated by the local planner based on the uniform linear motion model of the nonholonomic mobile robot. Each trajectory is scored according to the following cost function:

$$C_{BSC-DWA} = \alpha C_{obs} + \beta C_{goal} + \gamma C_{path} + \sigma C_{sc} \tag{14}$$

where C_{obs} is the sum of costs through which the trajectory passes; C_{goal} and C_{path} are the shortest distances from the endpoint of the simulated trajectory to the goal and the globally optimal path, respectively; and C_{sc} is the evaluation term for linear velocity and is used to evaluate the similarity between the sampling velocity and the shared control velocity. Inspired by previous work [34], C_{sc} is calculated as follows:

$$C_{sc} = \begin{cases} \dfrac{v_{sc} - v_{sample}}{v_{sc} - v_{\min}}, v_{sample} < v_{sc} \\ 0, v_{sample} = v_{sc} \\ \dfrac{v_{sample} - v_{sc}}{v_{\max} - v_{sc}}, v_{sample} > v_{sc} \end{cases} \tag{15}$$

where v_{sc} and v_{sample} are the shared control velocity and sampling velocity, respectively; and $v_{\min}$ and $v_{\max}$ are the minimum and maximum linear velocity, respectively. The score of each simulated trajectory can be obtained directly through the costmap according to Eqs. (14) and (15).

In this study, the mobile robot had a maximum linear velocity of 0.2 m s^{-1} and a maximum angular velocity of 0.5 m s^{-1}. The minimum linear and angular velocities of the robot were both 0 m s^{-1}. The linear and angular acceleration values of the robot were 0.2 and 0.4 m s^{-2}, respectively.

In conclusion, local collision-free trajectories are selected by minimizing the score CBSC-DWA of each sampling velocity, so that the control commands (v, ω) are to (1) move away from obstacles; (2) move toward the target; (3) stay close to the globally optimal path; and (4) move with a linear velocity close to the shared control velocity. During this process, any trajectories that might cause a collision are discarded.

2.5. Experimental paradigm

2.5.1. Overview of subjects, two-stage training, and experiments

Eight right-handed healthy subjects (5 males, 3 females; average age 25.13 ± 1.73 [mean ± standard deviation]) participated in the offline cue-based MI training and online cursor control training, and six out of the eight subjects participated in the online share control experiments since two subjects dropped out due to scheduling conflicts. All subjects were naïve to BCI training and the control tasks. Each subject was informed of the methods and procedures of this study. All procedures and protocols were in accordance with the Declaration of Helsinki.

In this study, we designed two-stage MI training (to be performed in the order of offline cue-based training and then online cursor control training) to take place before the online shared control experiments. In all training and experiments mentioned in this study, subjects completed MI tasks by imagining hand-grasping movements. Offline cue-based MI training was designed to obtain channel-frequency features for each

subject, and online cursor control training was designed to train the subjects' ability to continuously perform the MI tasks. Next, online shared control experiments were conducted to evaluate the performance of the proposed system. Both the training stages and the online shared control experiments were composed of several sessions, and each subject underwent a maximum of one session per day. Subjects were seated in a comfortable chair about 80 cm from an LCD screen and asked to stay relaxed during the session. Between each run of the session, the impedance of each electrode was measured to ensure that it remained below 10 kΩ during the active portion of the session in which the subjects were prompted to perform MI tasks.

2.5.2. Offline cue-based MI training

In this training stage, each subject was requested to participate in two sessions. Fig. 6(a) and Fig. 6(b) show the diagram and setup of offline cue-based training. Throughout all sessions, subjects were instructed to perform hand MI tasks, that is, left-hand MI for the left arrow, right-hand MI for the right arrow, both hands MI for the up arrow, and rest for the down arrow. The first session consisted of MI tasks with four directions (up, down, left, and right) and eight runs. In each run, subjects needed to perform 10 trials of MI tasks per direction with randomized order (40 trials in total). The second session consisted of MI tasks with two directions (up and down) and 10 runs. In each run, subjects needed to perform 10 trials of MI tasks per direction with randomized order (20 trials in total). Between two runs, subjects could rest for about 5 min to avoid fatigue.

Fig. 6(c) illustrates the offline training sequence protocol. The initial 3 s were set for subjects to relax. Following the initial 3 s, an arrow cue pointing to one randomized direction appeared in the center of the screen. Subjects were instructed to perform the corresponding MI task in the following 5 s. The trial ended with a black screen for 3 s to allow subjects to relax. Then, a new trial began under the same procedure.

2.5.3. Online cursor control training

In this training stage, each subject was requested to participate in one to three online virtual cursor control sessions based on their corresponding channel-frequency features. Fig. 6(d) and Fig. 6(e) show the diagram and the setup of online cursor control training. Throughout all sessions, users were instructed to perform both hands MI for the up arrow and rest for the down arrow, which made the virtual cursor rise and fall, respectively. Each session consisted of six runs. In each run, subjects performed 15 trials of MI tasks per direction with randomized order (30 trials in total). Subjects could rest for about 5 min between two runs.

Fig. 6(f) illustrates the sequence protocol of online cursor control training. The initial 2 s of each trial was set for subjects to relax. Following the initial 2 s, a pink bar appeared at the top or bottom edge of the screen randomly. Subjects were given 1 s to prepare before a pink cursor appeared at the center of the screen. Then subjects were instructed to execute MI tasks to hit the pink bar by moving the pink cursor within 8 s. Each trial could result in a hit (correct target), miss (incorrect target), or abort (target not reached, meaning a timeout) [35]. Both the bar and the cursor turned green when the result was a successful hit. The control task ended as soon as a clear result was produced in the set time or after a timeout. The trial ended with a black screen for 3 s to allow for subject relaxation. Then a new trial began under the same procedure.

The total correct rate (TCR) was calculated by dividing the number of hits by the number of total outcomes (including any abort outcomes). Only subjects with TCR higher than 80 % in any three consecutive runs of a session were allowed to participate in the online shared control experiments. Thus, the number of sessions conducted by subjects varied due to individual differences in training performance. Chance performance was estimated by collecting one session dataset for the cursor control task with electrodes plugged in but not connected to a human scalp.

2.5.4. Online shared control experiments

In this experiment, subjects interacted with the robot through MI to achieve a navigation task. As demonstrated in Fig. 7(a) and Fig. 7(b), the navigation field was defined as a rectangular corridor area (width: 310 cm; length: 790 cm) with four rectangular obstacles (1: width 16 cm, length 140 cm; 2: width 30 cm, length 71 cm; 3: width 30 cm, length 100 cm; 4: width 20 cm, length 25 cm). The start point (0.08 m,

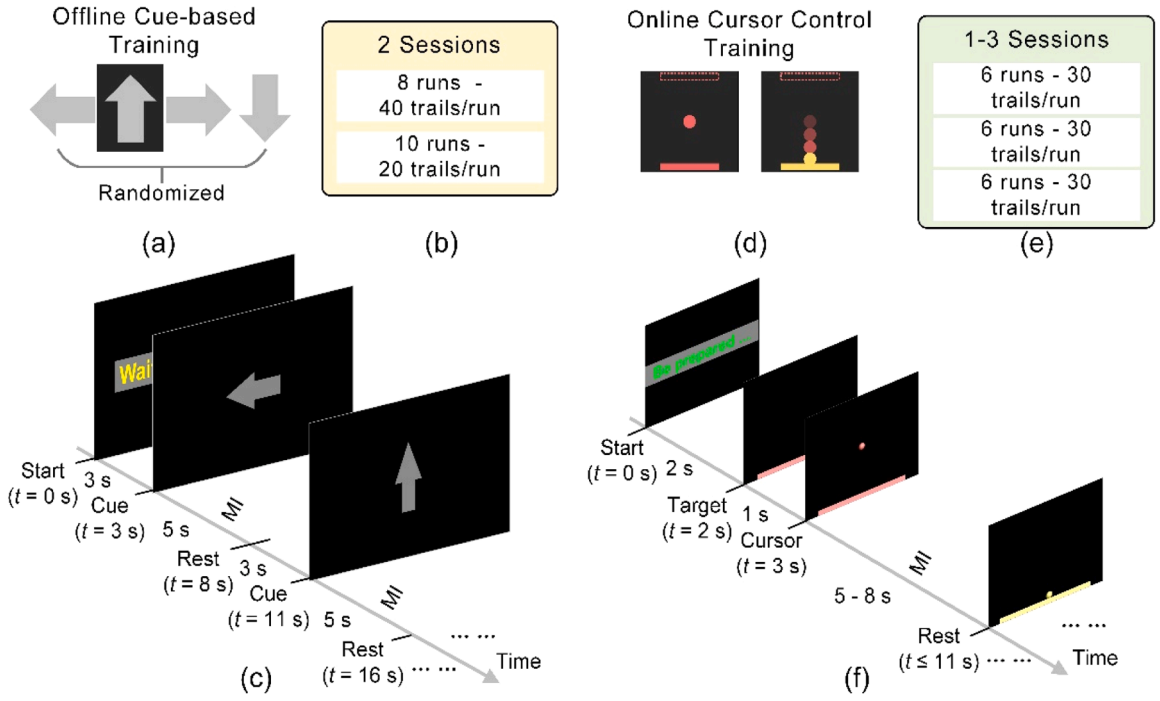

Fig. 6. Experimental framework for offline cue-based training and online cursor control training: (a) diagram, (b) experimental arrangement, and (c) experimental sequence protocol of offline cue-based training; (d) diagram, (e) experimental arrangement, and (f) experimental sequence protocol of online cursor control training.

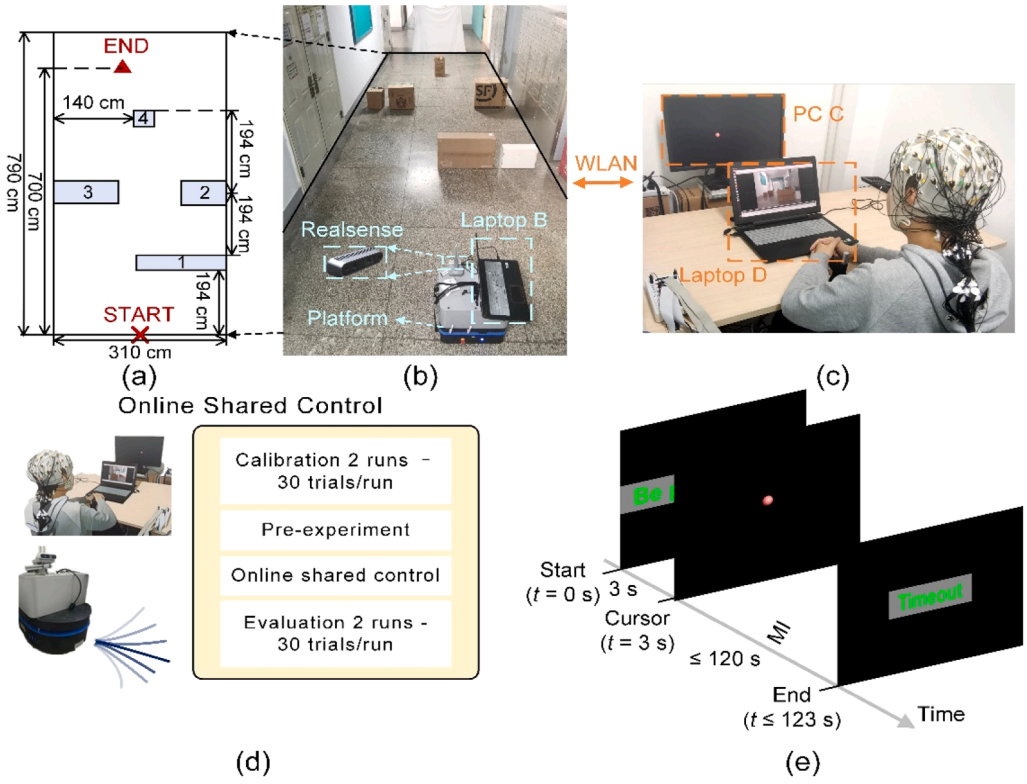

Fig. 7. Overview of online shared control experiments: (a) diagram of experimental field for the navigation tasks; (b) experimental field (a rectangular corridor area) and (c) experimental room for subjects to perform MI tasks; (d) experimental arrangement; and (e) sequence protocol of online shared control experiments.

0 m, 0) and end point (7 m, 0.5 m, $-\pi/2$) were fixed. The subject was seated in a normal room about 6 m away from the corridor (Fig. 7(c)). During navigation, industrial computer A was responsible for the control of the mobile platform, and laptop B was responsible for the environmental map construction, shared control, and local navigation. The virtual cursor was displayed on the screen of PC C. Video streams, provided by the RealSense camera, were shown to the subject on laptop D. The subjects were instructed to focus their attention on the environmental video feedback and avoid artifacts induced by saccades. Different modules were linked through a wireless local area network (WLAN).

Each subject was asked to participate in one to two sessions. Fig. 7(d) shows the experimental setup. The subjects performed two runs of MI cursor control tasks (the same as in the online cursor control training) both before and after the online shared control experiments to verify and evaluate their MI-based control level. The subjects also participated in a run of a continuous cursor control task for 60 s without a target bar before online control to get familiar with longtime continuous MI. Then four to seven runs of online shared control experiments were carried out (depending on the subject's level of fatigue). Subjects could rest for about 5–10 min between two runs.

As shown in Fig. 7(e), for the online shared control experiment, the subjects were prepared in the initial 3 s of each trial. Following the initial 3 s, the virtual cursor appeared in the center of the screen without a bar, and subjects were instructed to perform tasks (both hands MI to increase linear velocity and rest to decrease linear velocity) within a maximum of 120 s. When the subject performed both hands MI, the virtual cursor rose, and the speed of the robot increased. When the subject remained relaxed, the virtual cursor fell, and the speed of the robot decreased. Each run could result in success (reaching the ending point), failure, or abort (timeout).

Aside from online shared control experiments, autonomous navigation experiments were conducted with one session of eight runs in the same corridor. A constant linear velocity (0.1 m s^{-1}; half of v_{max}) was input to the BSC-DWA local planner instead of the shared control velocity signal. The mobile robot system achieved the same navigation task through SLAM, global path planner, and local navigation within a maximum of 120 s. Each run could result in success (reaching the ending point), failure, or abort (timeout).

The trajectory length of the mobile robot is one of the indicators reflecting the performance of the navigation method. In this study, we used an independent sample *t*-test to study whether the average trajectory length of autonomous navigation trials was significantly different from that of shared control trials.

3. Results

3.1. Two-stage MI training

The purpose of offline cue-based MI training was to obtain the most discriminative features of MI EEG before online control. A total of eight subjects participated in this training stage. Table 2 lists the subject-specific channel-frequency features selected according to the highest r^2 value [29] calculated between different MI tasks. The input of the AR model (see details in Section 2.2.1) was obtained from the selected channel, and the amplitude features of signals were extracted by the AR

Table 2
Channel-frequency features of BCI system.

Subject	Channel	Frequency (Hz)	MI task
A	C3/C4	9	Both hands/Relax
B	C3/C4	9	Both hands/Relax
C	C3/C4	12	Both hands/Relax
D	C3/C4	9	Both hands/Relax
E	C3/Cp4	9	Both hands/Relax
F	Cp3/C4	12	Both hands/Relax
G	C3/C4	12	Both hands/Relax
H	C3/C4	12	Both hands/Relax

model from the selected frequency band, which was uniquely identified by a center frequency and a bandwidth of 3 Hz. The distribution of the most discriminative frequency bands was consistent with the physiological characteristics of MI EEG.

In the online cursor control training, subjects learned to control the cursor based on MI tasks. When the subjects performed MI tasks, there were obvious characteristic changes in the energy frequency spectrum of EEG signals collected at different channels. Fig. 8(a) and Fig. 8(b) show the energy frequency spectrum of a single subject's EEG signals at C3 and C4 before and after cursor control training.

Compared with the relaxed state (red dotted line and red line), the energy of EEG at the Mu rhythm (8–13 Hz) decreased when the subjects imagined movement (blue dotted line and blue line). This phenomenon was consistent with ERD and indicated that brain activity was inhibited to a certain extent during MI tasks. Furthermore, the difference between the energy of EEG at the Mu rhythm in two mental states (dotted line: relaxed; solid line: both hands MI task state) was more pronounced after cursor control training (red: before training; blue: after training). This meant the changes in EEG amplitude features (used for generating continuous control signals) between the two states also increased after training, which indicated that the training improved the subject's capability of MI-based control.

To quantitatively assess the subject's level of control, we used the r^2 value, which represents the proportion of the variance associated with the class of the output signal [29]. Fig. 8(c) and Fig. 8(d) show a single subject's r^2 topography map of two mental states before training versus after training. The distribution of r^2 was concentrated around C3 and C4. The training led to a denser and larger r^2 value distribution and a significant increase in maximum r^2 values from 0.07 to about 0.25. Fig. 9 (a) shows maximum r^2 values in the online cursor control task before and after training.

After training, the average maximum r^2 value of subjects increased from 0.25 ± 0.10–0.52 ± 0.11. The distribution of the maximum r^2 value before and after training was significantly different (independent sample t-test, $p < 0.005$).

The subjects' control capability was evaluated in terms of percent valid correct (PVC) [9,13,35] and TCR. PVC was calculated as the number of hits divided by the total number of hits and misses (valid trials), and TCR was calculated by dividing the number of hits by the number of total outcomes (including any abort outcomes). As listed in Table 3, the online cursor control training through continuous BCI led to an increase in PVC from 78.25 % ± 14.71–97.13 % ± 3.40 %, which was similar to that in a previous study based on continuous BCI [9]. Fig. 9(b) shows the TCR of subjects in each session in the online cursor control task (N = 8). The average TCR of the eight subjects significantly improved from 53.37 % ± 16.25 % before training to 79.81 % ± 15.07 % after training (independent sample *t*-test; $p < 0.005$), which was also much higher than the random level (34 %). For beginners, there were also differences in the acceptance level of the BCI system and the ability to perform MI among different subjects. Subject A and subject E performed only one session, whereas subject B performed three sessions. The rest of the subjects (N = 5) performed two sessions to meet the requirement of TCR > 80 % in any three consecutive runs of a session.

3.2. Online shared control experiments

To demonstrate the proposed systems, online shared control experiments were performed. In the control process, the shared control weight α was dynamically adapted to the surrounding environment. Fig. 10(a) shows the global costmap offered by visual SLAM and Octomap with a resolution of 0.1 m. Three typical obstacle scenarios in the process are shown in Fig. 10(a), labeled as (1)–(3): (1) a C-shaped entrance, (2) a narrow passage, and (3) a simple obstacle. Fig. 10(b) shows the curve of the shared control weight in the whole navigation process. The weight changed dynamically according to the obstacles in the corridor. The closer the robot to the obstacle, the larger the sharing coefficient, so the BCI control signal worked with a lower weight.

As shown in Fig. 10(c), the shared control velocity was input into the proposed BSC-DWA method. The local planner sampled in a constrained velocity space, defined by Eq. (14), and generated simulated trajectories based on a uniform linear model in a series of simulated durations. These trajectories were evaluated according to Eq. (15), and the best one was selected by BSC-DWA (Fig. 10(c), left). The control pairs (v, ω) corresponding to the selected trajectory were then sent as control velocity commands. Fig. 10(d) indicates that the proposed BSC-DWA could consider the shared control velocity effectively since trajectories with low shared control cost values were selected most of the time.

Fig. 11 shows the curve of the linear velocity in the whole navigation process. As can be seen from Fig. 10(a), the robot was far away from the obstacle at the beginning, and the weight stayed at a low level (Fig. 10

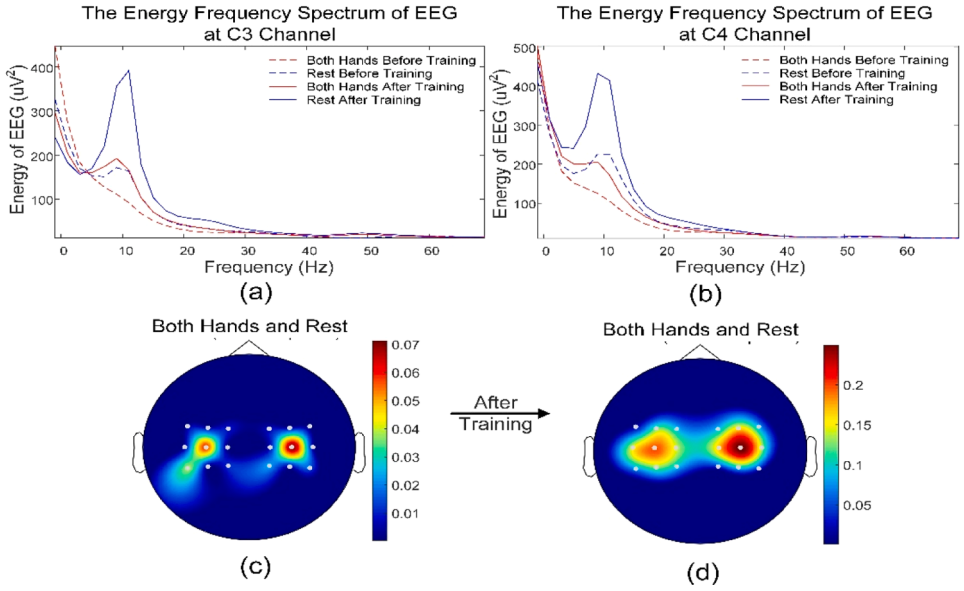

Fig. 8. MI modulation performance of offline cue-based MI training and online cursor control training. (a) The energy frequency spectrum of EEG signals at the C3 channel and (b) the energy frequency spectrum of EEG signals at the C4 channel were analyzed before and after training in different MI tasks. The topography map of r^2 in both hands MI versus relaxation MI was analyzed (c) before training and (d) after training.

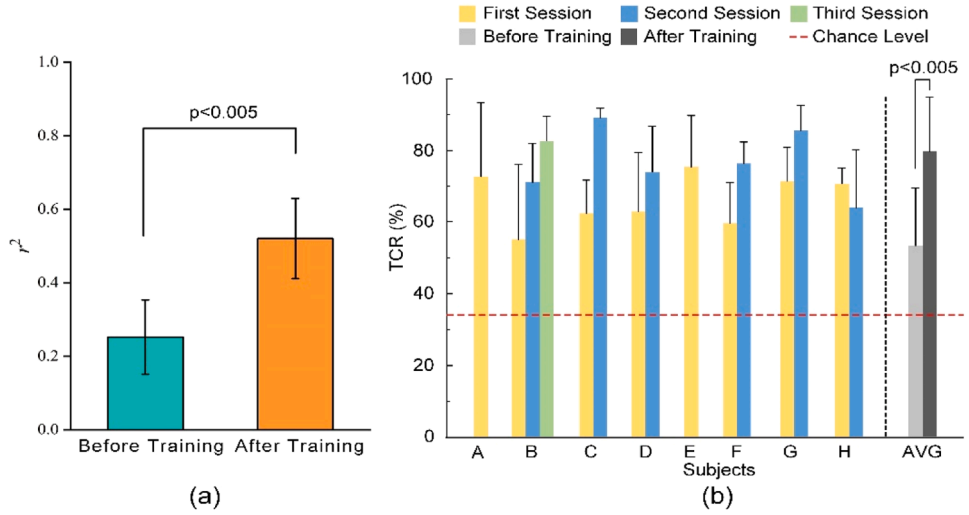

Fig. 9. BCI training performance of offline cue-based MI training and online cursor control training. (a) Maximum r^2 values in virtual cursor control task before and after training. (b) TCR of subjects in each session in virtual cursor control task.

Table 3
PVC of subjects in online cursor control tasks.

Research	Before training (%)	After training (%)
Our research	78.25 ± 14.71	97.13 ± 3.40
Meng et al.[9]	78.40 ± 7.00	Exceed 95.00

(b)). In the initial 15 s, the real velocity was consistent with the BCI velocity (Fig. 11). When the robot passed through the C-entrance (15–25 s), the weight increased dynamically. Meanwhile, there was a decreasing incline of BCI velocity, indicating that the subject participated in the control process effectively (~18 s). When the robot passed through the narrow passage (40–55 s), the shared control weight showed a sharp increase because the cost of environmental potential was relatively high. Thus, the proportion of EEG control signals was reduced. During this time, although the BCI module sent a high-level command (blue curve in Fig. 11), the decrease in shared control velocity (red curve) affected the real velocity (green curve). When the robot was to pass through the simple obstacle (67–80 s), the shared control weight increased slightly because of the approach to the obstacle and the wall. The subject also noticed the approaching obstacle and wall in the video feedback, so the BCI control signal decreased.

3.3. System integration performance

The proposed system achieved online navigation tasks in a corridor based on shared control and autonomous navigation. In each experiment, subjects had a maximum of 120 s to control. For online system performance, the update of the SLAM map took about 200 ms. After the

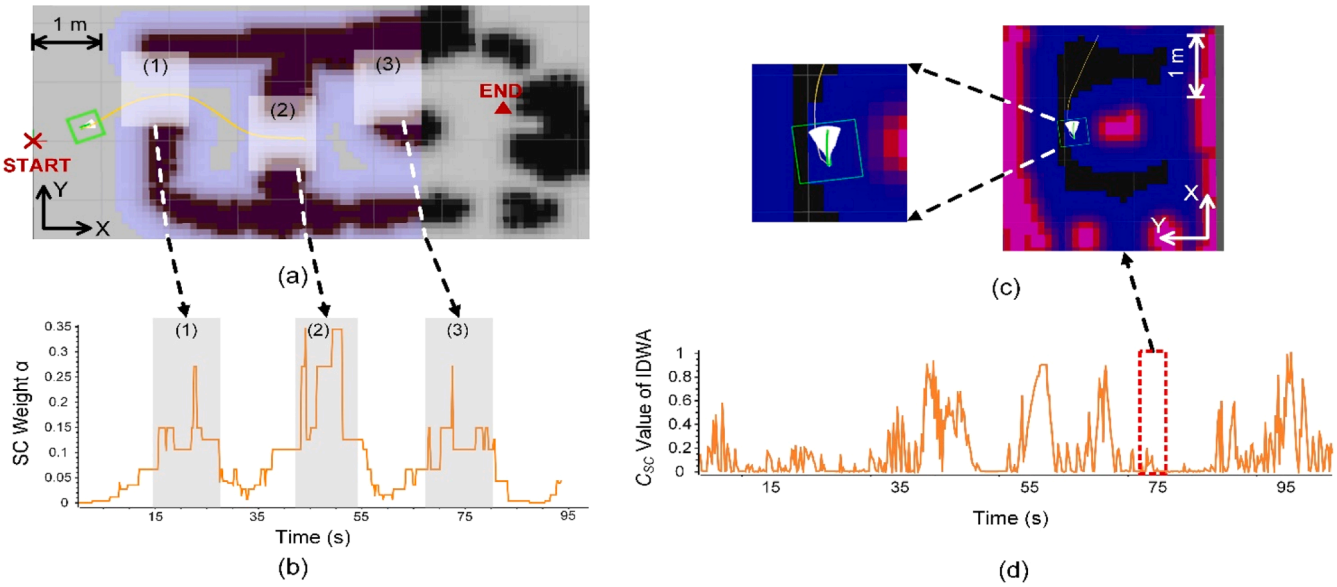

Fig. 10. Map construction, continuous shared control, and BSC-DWA local planning were realized in a real corridor. (a) A global costmap was constructed by visual SLAM and Octomap, and three typical obstacle scenarios were outlined: (1) a C-shaped entrance, (2) a narrow passage, and (3) a simple obstacle. The green rectangle represents the outline of the mobile robot. (b) The curve of the shared control weight. The weight dynamically adapted to the surrounding environment. (c) During the navigation task, BSC-DWA planned and scored simulated trajectories (left) when avoiding obstacles (right). (d) The curve of the shared control-based cost value of the BSC-DWA method. The red dotted box outlines the change in the shared control-based cost value when the robot was avoiding obstacles. The BSC-DWA planner executed the sampling and evaluation of velocity, taking the shared control velocity into consideration.

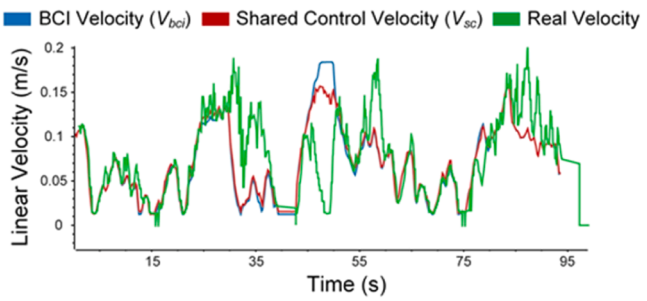

Fig. 11. Curves of linear velocities—including BCI velocity (blue), shared control velocity (red), and real velocity (green)—during the online shared control experiment.

map was initialized successfully, the BSC-DWA planning frequency of the online system was 5 Hz, and the continuous BCI module took about 50 ms to perform regression. Thus, the velocity planning control frequency of the entire shared control system was 5 Hz when the system was running normally.

To obtain the subjects' control performance, total experiment times, the number of successful navigations, the number of crash navigation, and the average duration of the successful experiment are listed in Table 4. As listed in Table 4, most of the subjects' attempts ended with success. The duration of success in shared control trials ranged from 87.00 ± 4.63–97.92 ± 6.05 s, higher than those in autonomous navigation trials at 85.77 ± 2.69 s. The length of trajectories in successful shared control trials ranged from 7.63 ± 0.03–7.81 ± 0.18 m, while the length of trajectories in successful autonomous navigation trials was 7.65 ± 0.09 m.

As shown in Fig. 12(a), in the two example trials, the robot was instructed to move from the initial configuration (0.08 m, 0 m, 0) to the desired configuration (7 m, 0.5 m, $-\pi/2$). Both shared control and autonomous navigation successfully avoided the obstacles and reached the target position. In detail, the shared control trajectory had a smaller turning radius as it went around the obstacle (1) than the autonomous navigation trajectory. Fig. 12(b) shows the statistical analysis of trajectory length. The average trajectory lengths of shared control trials and autonomous navigation trials were 7.67 ± 0.14 and 7.65 ± 0.09 m, respectively. An independent sample *t*-test was performed, and no significant difference was found between the average trajectory length of shared control trials and the average trajectory length of autonomous navigation trials. Fig. 12(c) illustrates the heat map of the start points (left) and end points (right) of trajectories generated by all subjects with a 1 cm resolution. Locations of the start points and end points are indicated by the color code ranging from blue to yellow according to normalized count (the count of each position divided by the maximum count of all positions). As demonstrated in Fig. 12(c), in the experiments, the start points were close to the same position, but the end points were more scattered around the ideal location. This result might be caused by the online visual SLAM method since the initial environment was unknown.

Table 4
Online navigation task performance.

Subject	Total times	Success times	Crash times	Duration of success (s)	Length of successful trajectories (m)
A	7	5	0	87.00 ± 4.63	7.63 ± 0.03
C	5	4	0	97.92 ± 6.05	7.64 ± 0.06
E	7	5	2	96.50 ± 14.94	7.65 ± 0.21
F	7	6	1	97.62 ± 7.19	7.65 ± 0.17
G	10	8	1	89.96 ± 9.38	7.81 ± 0.18
H	11	8	2	94.42 ± 6.39	7.64 ± 0.10
Autonomous navigation	8	8	0	85.77 ± 2.69	7.65 ± 0.09

Furthermore, we can see the performance of the mobile robot in the two example trials. Fig. 13 illustrates the change of kinematic parameters (linear velocity and angular velocity) of the system corresponding to the trajectory examples in Fig. 12(a). The autonomous navigation group used 0.1 m s^{-1} as the velocity input of BSC-DWA (the green line in Fig. 13(a)). According to Fig. 13(a), even though the instability of EEG influenced the control of linear velocity to some extent in the initial 20 s, the subject could still realize a successful navigation task using the proposed system. Fig. 13(b) demonstrates that the BSC-DWA method performed well in the control of angular velocity, both in shared control trials and autonomous navigation trials.

To analyze the effect of online shared control on subjects' control capability, the subjects were instructed to perform cursor control before and after online navigation tasks. According to the experimental design, all subjects were required to perform two runs before and after the shared control experiments to verify and evaluate control ability respectively. As listed in Table 5, before online shared control experiments, four out of six subjects had an average TCR higher than 80 %, and two subjects had average TCRs between 70 % and 80 %. After shared control, two out of six subjects maintained an average TCR higher than 80 %; three out of six subjects had average TCRs between 70 % and 80 %; and one out of six subjects had an average TCR of less than 70 %. After online shared control, three subjects (subjects A, C, and E) showed improvements in average TCR.

4. Discussion

The purpose of this study was to develop a continuous shared control approach combining continuous BCI control and robotic autonomous navigation for a mobile robot. To provide the disabled with daily assistance, various brain-actuated robotic devices have been developed. Most of these systems are driven by discrete BCI instructions and have shown great promise in different tasks, including reach and grasp tasks and navigation tasks [4,7,10,36,37]. In these studies, discrete commands (e.g., subtask selection or turning direction) are generated by well-trained decoders based on neurological modulation, which could be used for daily assistance. However, such discrete interactions do not allow users to realize continuous and natural control through EEG signals. From a practical point of view, a continuous interaction framework could enable users to precisely control a robotic device, which would be desirable [16]. Although the brain-driven mobile robot system provides a flexible approach, it is still challenging to control the robot directly depending on BCI. A shared control strategy combining BCI control and robotic autonomy provides effective assistance since it can avoid inappropriate commands generated by BCI. In addition, robotic autonomy can be an essential complement to enhance the perception and planning capability of mobile systems in daily scenarios, especially in unknown environments.

The present study demonstrated the proof of concept for a brain-actuated mobile robot system based on continuous MI BCI and autonomous navigation to achieve continuous shared control in a corridor environment. Subjects were able to achieve continuous control of the linear velocity of the robot through MI tasks. The mobile robot utilized visual SLAM to construct an environmental map and autonomous navigation to obtain safe trajectories. The shared controller dynamically adjusted the influence of continuous BCI and machine autonomy. In the online shared control experiments, all subjects were able to use the proposed system to complete the navigation task through continuous MI modulation and shared control. During the control process, well-trained subjects could participate in the continuous interaction effectively, and the shared control method dynamically adapted to changes in the

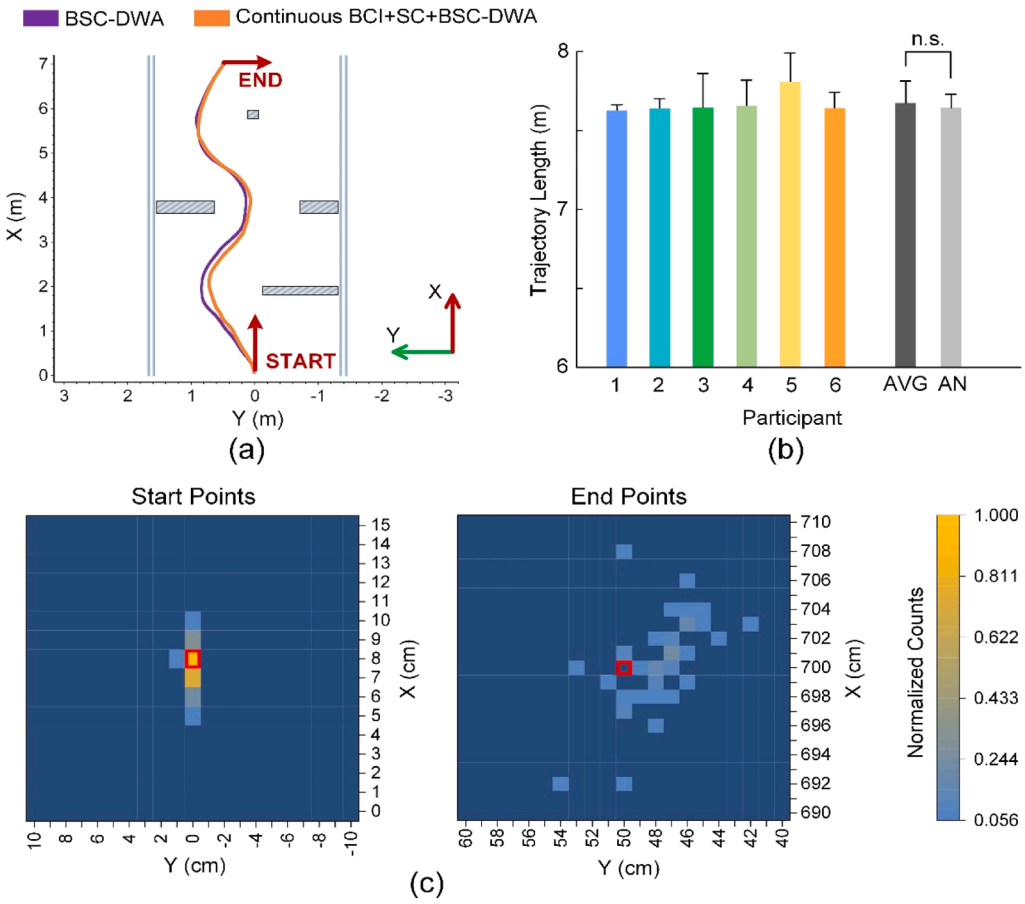

Fig. 12. Comparison of shared control performance and autonomous navigation performance in navigation tasks. (a) Example trajectories of the shared control trial (orange) and autonomous navigation trial (purple). The red arrows represent the initial start point (0.08 m, 0 m, 0) and end point (7 m, 0.5 m, $-\pi/2$) in the experiments. The direction setting was consistent with the coordinate system of ROS (right bottom). (b) Statistical data of trajectory length in the experiment. AN represents the autonomous navigation trials. (c) The distribution heat map of start points (left) and end points (right) of trajectories in the online experiments according to the normalized counts of appearance. The red rectangles outline the initial positions of the start and end points.

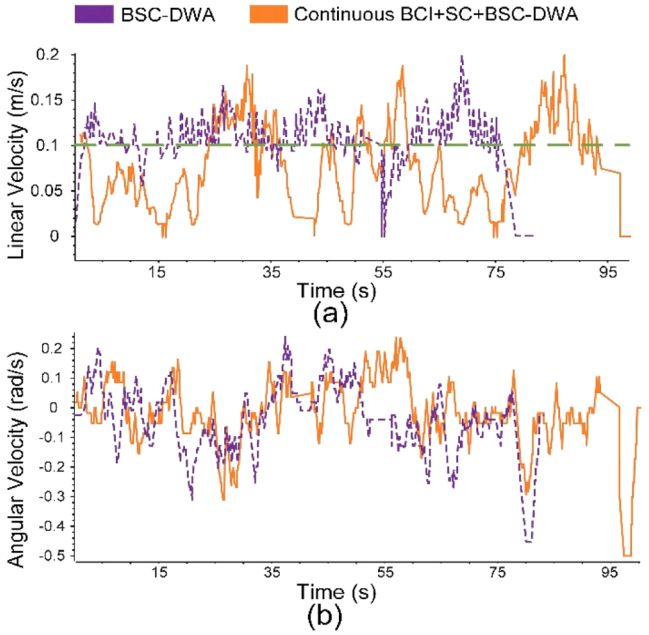

Fig. 13. The curves of (a) linear velocity and (b) angular velocity of the system correspond to the trajectory examples in Fig. 12(a). The orange curve represents the shared control trial, and the purple curve represents the autonomous navigation trial. The green line represents the constant velocity input of BSC-DWA in autonomous navigation trials (0.1 m s^{-1}).

surrounding environment. Experimental results verified the feasibility of realizing continuous BCI-based shared control for mobile robot systems, which is of great importance for daily application.

4.1. *Two-stage MI training evaluation*

ERD/ERS of SMR have been found to appear in the central sensorimotor area of the cerebral cortex during MI tasks and are directly related to movement, independent of visual or auditory stimuli [5,6]. Studies have shown that the spatial and frequency distribution of SMR differ between subjects when performing MI tasks [16]. To improve the performance of MI-based control for naïve users, we designed two-stage MI training, including offline cue-based training and online cursor control training. In the offline cue-based training stage, the most discriminative frequency bands of the subjects were concentrated in the Mu rhythm, which was consistent with the physiological characteristics of MI EEG. During the online cursor control training stage, feedback training was shown to significantly improve the distribution and values of r^2 as well as the PVC and TCR of naïve subjects.

Whereas BCI feedback plays a significant role in facilitating sensorimotor rhythm modulation [38], offline cue-based tasks can provide a measure of the subject's natural ability to modulate discriminative EEG patterns. ERD and ERS are considered to be the inhibition and activation of brain activities in specific frequency bands during MI tasks. According to our results, the energy frequency spectra of EEG signals at different electrode channels explained the ERD/ERS phenomenon (Fig. 8(a), (b)). The modulation effect of the SMR rhythm in the MI task was quantified by the numerical change and the scalp distribution topography of r^2. In addition, ERD/ERS became more pronounced over time, indicating that feedback training could promote cognitive processes and might play an important role in BCI control.

Table 5
Performance of subjects in cursor control tasks before and after online shared control experiments.

Subject	Training runs	TCR before online shared control (%)			TCR after online share control (%)		
		Run 1	Run 2	Average	Run 1	Run 2	Average
A	10	73.07	80.77	76.92	80.77	76.92	78.85
C	26	84.62	80.77	82.70	88.46	84.62	86.54
E	18	73.07	76.92	75.00	76.92	80.77	78.85
F	10	88.46	84.62	86.54	65.38	80.77	73.08
G	18	80.77	88.46	84.62	61.54	76.92	69.23
H	18	92.31	84.62	88.47	80.77	84.62	82.70

For naïve individuals, friendly and progressive training is very important. Staged training is an effective approach to improve the performance of both subjects and the BCI system [13]. Percent accuracy was determined for two different criteria: PVC [9,13] and TCR. In our study, the effect of training was similar to the advanced level reported in [9], a continuous BCI study based on the regression method. Meanwhile, during the training process of one of the subjects, the TCR decreased (Fig. 9(b), subject H). All of the subjects had higher TCRs than the random level (34 %). After training, seven out of eight subjects achieved over 80 % accuracy in cursor control tasks in three consecutive runs in the same session and were qualified to conduct online shared control experiments. In the online cursor control experiments, we observed significant differences in the capability of different subjects to master online cursor control through SMR modulation. According to the review of subjects, we also noticed that the mental state of subjects may have an effect on experimental performance, which could be studied in future works. Both fatigue and unfamiliarity with tasks could be a challenge for naïve users to learn to modulate SMR. As reported in the literature, appropriate behavior intervention (e.g., mindfulness) could be helpful to enhance the performance of continuous BCI training [39,40].

In all, the two-stage training enabled subjects to perform continuous control through neural modulation. In addition, inspired by continuous cursor pursuit tasks, which have been proven to enhance the learning performance of continuous control [13,14], a 60 s cursor control task without a target was utilized as a guide before online shared control. As instructed in the flow of online shared control experiments, the guide task works as an analog of continuous control in daily application. The effect and design of such a training paradigm should be further investigated in future work.

4.2. Role of shared control and autonomous navigation

It is still a challenge to drive robotic devices directly through BCI because this puts a large mental burden on users. To improve the performance of brain-actuated systems, the shared control strategy has been widely discussed and investigated [3,19–21]. Generally, a shared control architecture is conceived to integrate user commands (generated by cognitive intention) and robotic autonomy [17]. In this article, we designed a continuous and adaptive shared control strategy combining continuous BCI and autonomous navigation. During the online shared control experiments, the subjects interacted with a mobile robot to accomplish navigation tasks in an unknown corridor environment. The subject and the robot played different roles during the shared control process. The intelligent mobile robot module was responsible for sensing the surrounding environment (map construction and localization) and planning collision-free trajectories. The subject was in charge of continuously controlling the linear velocity of the robot depending on MI tasks.

For a shared control strategy, one approach is to realize continuous adaptive assistance based on the surrounding environment. To date, several types of shared control arbitrators have been explored in BCI systems, including explicit linear combinations [3,19] and other fusion rules (e.g., probability-based methods [21]). However, the design of the current linear arbitrator is fixed or relies on experience, which limits the flexibility of the arbitrator. To take advantage of the obstacle information in the global map, we presented the weight of shared control based on the environmental cost field, expressed by Eq. (9). The weight reflects the corresponding relationship of cost value between the current position of the mobile robot and surrounding obstacles. This approach tends to use shared control when the distance between the obstacle and the robot is less than the expansion distance. Experimental results showed that the sharing weight could dynamically adapt to changes in the distances between the robot and surrounding obstacles during the control process. When the robot moved close to obstacles, the weight increased gradually (approximate exponential tendency). This change was consistent with the theoretical design.

For local autonomous navigation, it is essential to consider shared control velocity during trajectory evaluation. The traditional DWA method could plan safe and reachable trajectories with nonholonomic constraints [25,33]. In this work, the BSC-DWA method integrating the shared control velocity cost was used to conduct velocity sampling, trajectory simulation, and evaluation. The BSC-DWA planner was also considered to provide an implicitly shared intelligence to plan safe and reachable trajectories and respond to shared control output simultaneously. The results indicated that BSC-DWA achieved planning comprehensively and was able to select velocities that corresponded to shared control output. As shown in Fig. 11, after training, subjects were able to successfully complete online shared control using continuous BCI. In the final stage, when the robot reached the vicinity of the target point, the BSC-DWA method automatically completed the control of position and pose.

In general, the online shared control experiments verified the validity of the proposed method integrating continuous BCI, adaptive shared control, autonomous navigation, and visual SLAM. The proposed BSC-DWA achieved comprehensive planning for collision-free navigation based on continuous shared control.

4.3. Integrated system evaluation

The brain-driven mobile robot is a typical and important BCI system that provides a flexible and extensible approach to daily assistance. In many studies, brain-driven mobile platforms—including wheelchairs [4,33,41], mobile robots [7,10,16,42], and high-speed vehicles [43]—have been explored and investigated. These studies have shown great promise in coordination and shared autonomy between humans and robots. However, there are still limits to realizing continuous BCI control of such a comprehensive system. In the present study, we proposed an intelligent brain-driven mobile robot system, which enables users to conduct

continuous shared control through BCI. Visual SLAM method and autonomous navigation expand the possible uses for the system. The results of online shared control experiments proved the feasibility of the system in a navigation task.

Regarding navigation performance, all of the subjects were able to control the mobile robot system based on MI and shared control, and most of their attempts ended with success (Table 4). We noticed that the duration of the subjects' successful trials was longer than the duration of autonomous navigation. Even though the instability of EEG somewhat influenced the control of linear velocity (e.g., the initial 20 s in Fig. 13 (a)), the subjects could still succeed in navigation tasks using the proposed system. This can be seen as evidence that the comprehensive system provides subjects with effective assistance in navigation tasks. Besides, the perceptive ability of the robot system is valuable for unknown environments. By extending the visual SLAM method based on ORB-SLAM2, the system could autonomously construct a dense environmental map (~200 ms for updating the local map). In the control process, the regression of EEG took about 50 ms and the planning frequency of BSC-DWA was 5 Hz. Robotic autonomy provides an effective way to improve the efficiency and extend the scope of application of EEG-based BCI systems. Compared with similar work [10], our system could realize more continuous and precise control of linear velocity in a shorter response time.

Regarding the influence of online shared control, we investigated subjects' performance in the same cursor control tasks before and after shared control. Directly controlling the movement of the mobile robot through EEG might easily cause fatigue for subjects. In the present study, the proposed continuous shared control strategy directly influenced the velocity of the mobile robot through EEG, and the robotic autonomy provided effective assistance during this process, achieving a reasonable balance between continuous velocity control and user workload. Moreover, the performance of three subjects on TCR was improved after the online shared control experiment, which indicated that practicing long-time continuous BCI control could enhance MI performance [13].

In general, all the subjects were able to control the robot through EEG continuously, which verifies the effectiveness of our proposed shared control method. The trained subjects were already familiar with the continuous BCI control, and they were able to master cursor control and complete continuous online control tasks. To improve the shared assistance of robotic intelligence, enhancing the robot's understanding and inference of user intention might warrant exploration in future work [44].

4.4. Limitations and future work

Despite the superior performance of the proposed system, further investigation should be conducted. The performance of the current continuous BCI control system should be investigated in more complex and larger-scale scenarios (e.g., long corridor, corner, and outdoor) to better simulate environments encountered in daily life. In addition, since we only recruited healthy subjects to verify the proposed system, studies should be conducted to investigate the performance of the system with disabled subjects.

Future work should be carried out considering the following aspects. First, paralyzed participants should be recruited for our subsequent research. Feedback from disabled subjects will be of great value to evaluate and improve the proposed system for daily application. In addition, enhancing the recognition and inference of human intention could greatly improve the shared control strategy, so the modeling of human intention and environment is worthy of exploration (e.g., Markov decision process, probabilistic-based inference model). Finally, the perception and planning performance of robots should be improved. Dynamic SLAM provides a flexible solution to complex workspaces, and the combination of a mobile robot and robotic arm would also extend the application of our system.

5. Conclusion

In this article, we proposed a continuous shared control strategy combining continuous BCI and autonomous navigation for the brain-actuated mobile robot system. The adoption of BCI and shared control enabled subjects to drive a mobile robot continuously to complete a navigation task in an unknown corridor. The visual SLAM and path planning methods were utilized for environmental perception and navigation. We designed a BSC-DWA planner to generate safe and collision-free trajectories considering obstacles and shared control signals. Two-stage training enabled naïve subjects to learn to perform continuous control through neural modulation in a limited number of training sessions. Online shared control experiments demonstrated that all well-trained subjects were able to complete the navigation tasks with the assistance of a shared control strategy. The experimental results indicated the feasibility and promise of continuous shared control based on MI and autonomous navigation for daily assistance.

CRediT authorship contribution statement

Baoguo Xu and Deping Liu designed the study, analyzed the data, and wrote the manuscript. Deping Liu set up the experiment platform. Deping Liu and Muhui Xue performed the experiment. Minmin Miao, Cong Hu, and Aiguo Song reviewed and edited the manuscript. All authors read and approved the final manuscript.

Declaration of Competing Interest

The authors declare that the research was conducted in the absence of any commercial or financial relationships that could be construed as a potential conflict of interest.

Appendix A. Supporting information

Supplementary data associated with this article can be found in the online version at doi:10.1016/j.csbj.2023.07.033.

References

[1] Vansteensel MJ, et al. Fully implanted brain-computer interface in a locked-in patient with ALS. Nov. 24 N Engl J Med 2016;375(21):2060–6. https://doi.org/10.1056/NEJMoa1608085.
[2] McFarland DJ, Sarnacki WA, Wolpaw JR. Electroencephalographic (EEG) control of three-dimensional movement. Art no. 036007 J Neural Eng 2010;7(3). https://doi.org/10.1088/1741-2560/7/3/036007.
[3] Xu Y, et al. Shared control of a robotic arm using non-invasive brain-computer interface and computer vision guidance. Robot Auton Syst 2019;115:121–9. https://doi.org/10.1016/j.robot.2019.02.014.
[4] Leeb R, Tonin L, Rohm M, Desideri L, Carlson T, Millan JdR. Towards independence: a BCI Telepresence robot for people with severe motor disabilities. Proc IEEE . 2015;103(6):969–82. https://doi.org/10.1109/jproc.2015.2419736.
[5] Li Z, Zhao S, Duan J, Su C-Y, Yang C, Zhao X. Human cooperative wheelchair with brain-machine interaction based on shared control strategy. IEEE/ASME Trans Mechatron 2017;22:185–95. https://doi.org/10.1109/tmech.2016.2606642.
[6] Pfurtscheller G, Neuper C, Flotzinger D, Pregenzer M. EEG-based discrimination between imagination of right and left hand movement. Electroencephalogr Clin Neurophysiol 1997;103(6):642–51. https://doi.org/10.1016/s0013-4694(97)00080-1.
[7] Pfurtscheller G, da Silva FHL. Event-related EEG/MEG synchronization and desynchronization: basic principles. Clin Neurophysiol 1999;110(11):1842–57. https://doi.org/10.1016/s1388-2457(99)00141-8.
[8] Kuhner D, et al. A service assistant combining autonomous robotics, flexible goal formulation, and deep-learning-based brain-computer interfacing. Robot Auton Syst 2019;116:98–113. https://doi.org/10.1016/j.robot.2019.02.015.
[9] Meng J, Zhang S, Beyko A, Olsoe J, Baxter B, He B. Noninvasive electroencephalogram based control of a robotic arm for reach and grasp tasks (vol 6, 38565, 2016). Apr. 15 Sci Rep 2020;10(1). https://doi.org/10.1038/s41598-020-63070-z.
[10] Li J, Li Z, Feng Y, Liu Y, Shi G. Development of a human-robot hybrid intelligent system based on brain teleoperation and deep learning SLAM. IEEE Trans Autom Sci Eng 2019;16(4):1664–74. https://doi.org/10.1109/tase.2019.2911667.
[11] McFarland DJ, Wolpaw JR. EEG-based communication and control: Speed-accuracy relationships. Appl Psychophysiol Biofeedback 2003;28(3):217–31. https://doi.org/10.1023/a:1024685214655.

[12] Wolpaw JR, McFarland DJ. Control of a two-dimensional movement signal by a noninvasive brain-computer interface in humans. Dec. 21 Proc Natl Acad Sci 2004; 101(51):17849–54. https://doi.org/10.1073/pnas.0403504101.
[13] Edelman BJ, et al. Noninvasive neuroimaging enhances continuous neural tracking for robotic device control. Jun. 19 Sci Robot 2019;4(31). https://doi.org/10.1126/scirobotics.aaw6844.
[14] Suma D, Meng J, Edelman BJ, He B. Spatial-temporal aspects of continuous EEG-based neurorobotic control. Art no. 066006 J Neural Eng 2020;17(6). https://doi.org/10.1088/1741-2552/abc0b4.
[15] Deng X, Yu ZL, Lin C, Gu Z, Li Y. A Bayesian shared control approach for wheelchair robot with brain machine interface. IEEE Trans Neural Syst Rehabil Eng 2020;28(1):328–38. https://doi.org/10.1109/tnsre.2019.2958076.
[16] Tonin L, Bauer FC, Millan J d R. The role of the control framework for continuous teleoperation of a brain-machine interface-driven mobile robot. IEEE Trans Robot 2020;36(1):78–91. https://doi.org/10.1109/tro.2019.2943072.
[17] Selvaggio M, Cognetti M, Nikolaidis S, Ivaldi S, Siciliano B. Autonomy in physical human-robot interaction: a brief survey. IEEE Robot Autom Lett 2021;6(4): 7989–96. https://doi.org/10.1109/lra.2021.3100603.
[18] Duan J, Li Z, Yang C, Xu P. Shared control of a brain-actuated intelligent wheelchair, in 11th World Congress on Intelligent Control and Automation, Shenyang. Peoples R China 2014:341–6.
[19] Xu Y, Zhang H, Cao LF, Shu XK, Zhang DG. A shared control strategy for reach and grasp of multiple objects using robot vision and noninvasive brain-computer interface. IEEE Trans Autom Sci Eng 2022;19(1):360–72. https://doi.org/10.1109/tase.2020.3034826.
[20] Deng XY, Yu ZL, Lin CG, Gu ZH, Li YQ. Self-adaptive shared control with brain state evaluation network for human-wheelchair cooperation. Art no. 045005 J Neural Eng 2020;17(4). https://doi.org/10.1088/1741-2552/ab937e.
[21] Cao LF, Li GY, Xu Y, Zhang H, Shu XK, Zhang DG. A brain-actuated robotic arm system using non-invasive hybrid brain- computer interface and shared control strategy. Art no. 046045 J Neural Eng 2021;18(4). https://doi.org/10.1088/1741-2552/abf8cb.
[22] S.Y. Liu et al., Mind Controlled Vehicle Based on Lidar SLAM Navigation and SSVEP Technology, in *9th IEEE International Winter Conference on Brain-Computer Interface (BCI)*, Korea Univ Inst Artificial Intelligence, ELECTR NETWORK, Feb. 22–24 2021, pp. 294–297.
[23] J. Park, J.W. Choi, S. Jo, and Ieee, A SLAM Integrated Hybrid Brain-Computer Interface for Accurate and Concise Control, in *7th International Winter Conference on Brain-Computer Interface (BCI)*, Korea Univ, Res Ctr Brain & Artificial Intelligence, Gangwon, SOUTH KOREA, Feb. 18–20 2019, pp. 78–82.
[24] Yuan Y, Su W, Li Z, Shi G. Brain-computer interface-based stochastic navigation and control of a semiautonomous mobile robot in indoor environments. IEEE Trans Cogn Dev Syst 2019;11(1):129–41. https://doi.org/10.1109/tcds.2018.2885774.
[25] Fox D, Burgard W, Thrun S. The dynamic window approach to collision avoidance. IEEE Rob Autom Mag 1997;4(1):23–33. https://doi.org/10.1109/100.580977.
[26] M. Seder, I. Petrovic, and Ieee, Dynamic window based approach to mobile robot motion control in the presence of moving obstacles, in IEEE Int. Conf. Robot. Autom, Rome, ITALY, 2007, pp. 1986–1991.
[27] M. Missura, M. Bennewitz, and Ieee, Predictive Collision Avoidance for the Dynamic Window Approach, in IEEE Int. Conf. Robot. Autom, Montreal, CANADA, 2019, pp. 8620–8626.
[28] McFarland DJ, Wolpaw JR. Sensorimotor rhythm-based brain-computer interface (BCI): model order selection for autoregressive spectral analysis. J Neural Eng 2008;5(2):155–62. https://doi.org/10.1088/1741-2560/5/2/006.
[29] Schalk G, McFarland DJ, Hinterberger T, Birbaumer N, Wolpaw JR. BCI2000: a general-purpose, brain-computer interface (BCI) system. IEEE Trans Biomed Eng 2004;51(6):1034–43. https://doi.org/10.1109/tbme.2004.827072.
[30] Tang J, Liu Y, Hu D, Zhou Z. Towards BCI-actuated smart wheelchair system. Aug. 20 BioMed Eng OnLine 2018;17. https://doi.org/10.1186/s12938-018-0545-x.
[31] Mur-Artal R, Tardos JD. ORB-SLAM2: an open-source SLAM system for monocular, stereo, and RGB-D cameras. IEEE Trans Robot 2017;33(5):1255–62. https://doi.org/10.1109/tro.2017.2705103.
[32] E. Marder-Eppstein, E. Berger, T. Foote, B. Gerkey, K. Konolige, and Ieee, The Office Marathon: Robust Navigation in an Indoor Office Environment, in IEEE Int. Conf. Robot. Autom, Anchorage, AK, 2010, pp. 300–307.
[33] Lopes AC, Rodrigues J, Perdigao J, Pires G, Nunes UJ. A new hybrid motion planner applied in a brain-actuated robotic wheelchair (Mag) IEEE Robot Autom 2016;23(4):82–93. https://doi.org/10.1109/mra.2016.2605403.
[34] de Lima DA, Victorino AC. A hybrid controller for vision-based navigation of autonomous vehicles in urban environments. IEEE Trans Intell Transp Syst 2016;17 (8):2310–23. https://doi.org/10.1109/tits.2016.2519329.
[35] Meng J, Streitz T, Gulachek N, Suma D, He B. Three-dimensional brain-computer interface control through simultaneous overt spatial attentional and motor imagery tasks. IEEE Trans Biomed Eng 2018;65(11):2417–27. https://doi.org/10.1109/tbme.2018.2872855.
[36] Li T, Hong J, Zhang J, Guo F. Brain-machine interface control of a manipulator using small-world neural network and shared control strategy. Mar. 15 J Neurosci Methods 2014;224:26–38. https://doi.org/10.1016/j.jneumeth.2013.11.015.
[37] Han X, Lin K, Gao S, Gao X. A novel system of SSVEP-based human-robot coordination. Art no. 016006 J Neural Eng 2019;16(1). https://doi.org/10.1088/1741-2552/aae1ba.
[38] Ono T, Kimura A, Ushiba J. Daily training with realistic visual feedback improves reproducibility of event-related desynchronisation following hand motor imagery. Clin Neurophysiol 2013;124(9):1779–86. https://doi.org/10.1016/j.clinph.2013.03.006.
[39] Perdikis S, Tonin L, Saeedi S, Schneider C, Millan J d R. The cybathlon BCI race: successful longitudinal mutual learning with two tetraplegic users. Art no. e2003787 PLoS Biol 2018;16(5). https://doi.org/10.1371/journal.pbio.2003787.
[40] Stieger JR, Engel S, Jiang H, Cline CC, Kreitzer MJ, He B. Mindfulness improves brain-computer interface performance by increasing control over neural activity in the alpha band. Cereb Cortex 2021;31(1):426–38.
[41] Iturrate I, Antelis JM, Kuebler A, Minguez J. A noninvasive brain-actuated wheelchair based on a P300 neurophysiological protocol and automated navigation. IEEE Trans Robot 2009;25(3):614–27. https://doi.org/10.1109/tro.2009.2020347.
[42] Millan JD, Renkens F, Mourino J, Gerstner W. Noninvasive brain-actuated control of a mobile robot by human EEG. IEEE Trans Biomed Eng 2004;51(6):1026–33. https://doi.org/10.1109/tbme.2004.827086.
[43] Lu Y, Bi L. Combined lateral and longitudinal control of EEG signals-based brain-controlled vehicles. IEEE Trans Neural Syst Rehabil Eng 2019;27(9):1732–42. https://doi.org/10.1109/tnsre.2019.2931360.
[44] Jain S, Argall B. Probabilistic human intent recognition for shared autonomy in assistive robotics. Art no. 2 ACM Trans Hum Robot Inter 2020;9(1). https://doi.org/10.1145/3359614.